Monomerizing the ultrabright AausFP1 yields mBiyu for advanced imaging across challenging bacterial and mammalian cells

Yu Yan[1], Yiqing Shen[1,5], Chaoying Peng[1,5], Xinyu Wang[1], Xiao Lin[3], Xiaodong Ye[4], Jiajia Wang[1], Sijing Zhang[1], Hui Wang[1,2], Xianghui Ou[1], Ying Li[3], Shishen Du[3], Quan Chen[1,2*], XinxingYang[1,2*]

1. MOE Key Laboratory for Cellular Dynamics, Center for Advanced Interdisciplinary Science and Biomedicine of IHM, Hefei National Research Center for Interdisciplinary Sciences at the Microscale, Division of Life Sciences and Medicine, University of Science and Technology of China, Hefei, 230026, China

2. Anhui Basic Discipline Research Center of Artificial Intelligence Biotechnology and Synthetic Biology, Hefei. China

3. State Key Laboratory of Metabolism and Regulation in Complex Organisms, College of Life Sciences, Wuhan University, Wuhan, China

4. Department of Chemical Physics, Hefei National Research Center for Physical Sciences at the Microscale, University of Science and Technology of China, Hefei, Anhui 230026, China

5. These authors contributed equally: Yiqing Shen and Chaoying Peng

* E-mail: chenquan@ustc.edu.cn, xinxingyang@ustc.edu.cn

Fluorescent proteins (FPs) enable noninvasive visualization of cellular processes. For advanced imaging applications, high molecular brightness is a key determinant of FP performance. AausFP1 is a newly discovered, ultrabright green FP derived from *Aequorea cf. australis* that shares low sequence identity with widely used avGFP. It combines a near-unity quantum yield with a high extinction coefficient, yet its native oligomerization and poor solubility limits use as a fusion tag. Here we report mBiyu, a monomeric AausFP1 engineered by structure-guided interface disruption followed by iterative directed evolution. mBiyu preserves AausFP1's high quantum yield, matures rapidly, and tolerates demanding conditions such as aldehyde fixation and protease digestion, enabling its use in expansion microscopy. In mammalian cells and across diverse prokaryotes, mBiyu behaves as a monomer and delivers strong fusion performance, including challenging bacteria such as *Staphylococcus aureus*, *Mycobacterium smegmatis*, and *Deinococcus radiodurans*. These properties make mBiyu a robust tag for long time-lapse and high-resolution imaging in difficult organisms and demanding conditions.

Introduction

Genetically encoded fluorescent proteins (FPs) are indispensable tools for visualizing molecular processes in cells and organisms. Since the discovery of green fluorescent protein (GFP) from *Aequorea Victoria*[1], extensive protein engineering has produced a broad palette of variants with improved brightness, maturation rate, and stability, enabling increasingly sophisticated imaging modalities[2-4]. Despite substantial progress, most widely used FPs descend from a small set of scaffolds, constraining further diversification. Recently, new fluorescent proteins from diverse species are expanding the available toolkit. Two proteins, in particular, have attracted attention: StayGold[5], derived from the jellyfish *Cytaeis uchidae*, which exhibits exceptional photostability, and AausFP1[6], isolated from *Aequorea cf. australis*, which combines near-unity quantum yield (~0.97) with an exceptionally high extinction coefficient (~170,000 M^{-1} cm^{-1}), making it the brightest green FP reported to date.

Since a high signal-to-noise ratio is essential for high-resolution and long-duration imaging, the high brightness is always the "Holy Grail" of the FP engineering[7]. AausFP1 shares only 53% sequence identity with *Aequorea victoria* GFP (avGFP) and produces extremely strong signal in both *Escherichia coli* (*E. coli*) and mammalian cells[6]. However, it natively forms dimer and higher-order oligomers, leading to poor solubility and aggregation of the fused proteins, limiting its utility as a fusion tag and in biosensor applications.

Here, we sought to monomerize AausFP1 by combining structure-guided interface redesign with iterative directed evolution to enable its broad application. Using rationally designed mutagenesis to disrupt the dimer interface and random mutagenesis to recover the fluorescence, we generated mBiyu ("Biyu"; 碧玉, jasper in Chinese), a bright monomeric derivative of AausFP1 containing fifteen substitutions. mBiyu behaves as a monomer in living Hela and *E. coli* cells while retaining high intrinsic brightness comparable to leading monomeric green FPs, including mNeonGreen (mNG)[8] and mBaojin[9] (a monomeric StayGold-family FP). It also exhibits rapid maturation and robust chemical and thermal stability. Notably, mBiyu performs exceptionally well across multiple prokaryotes, making it a strong candidate for microbial studies; for example, in *Staphylococcus aureus* (*S. aureus*, a famous pathogen) and *Mycobacterium smegmatis* (*M. smegmatis*, a model bacterium to study *Mycobacterium tuberculosis*), challenging hosts in which few FPs function reliably, mBiyu fusions outperform commonly used GFPs and enable long time-lapse imaging with high signal. Taken together, these results establish mBiyu as a bright, stable, and versatile monomeric green FP suited to advanced live- and fixed-cell imaging applications.

Results

Identification and mutation of key interactive residues on the AausFP1 dimeric interface

To generate a monomeric AausFP1, we first examined the dimeric interface in the crystal structure of AausFP1 (PBD 6S67, Fig. 1a). Structural inspection in PyMOL[10] revealed eight residues potentially stabilizing intermolecular association by hydrophobic or electrostatic interactions (C147, Y149, K160, V166, Y196, H198, R223 and K228, Fig. 1b, Supplementary Table 1). We therefore preformed alanine or arginine replacement at these residues to block the polar interactions or hydrophobic contacts at the interface[11] (Methods, Fig. S1a). Among the resulting variants, C147R, V166R and H198A each produced a monomeric band on the pseudo-native SDS-PAGE, although residual dimeric and oligomer bands remained detectable (Fig. S1b). We next combined these substitutions to create a minimal triple mutant, C147R/V166R/H198A, hereafter referred to as mAaus. mAaus

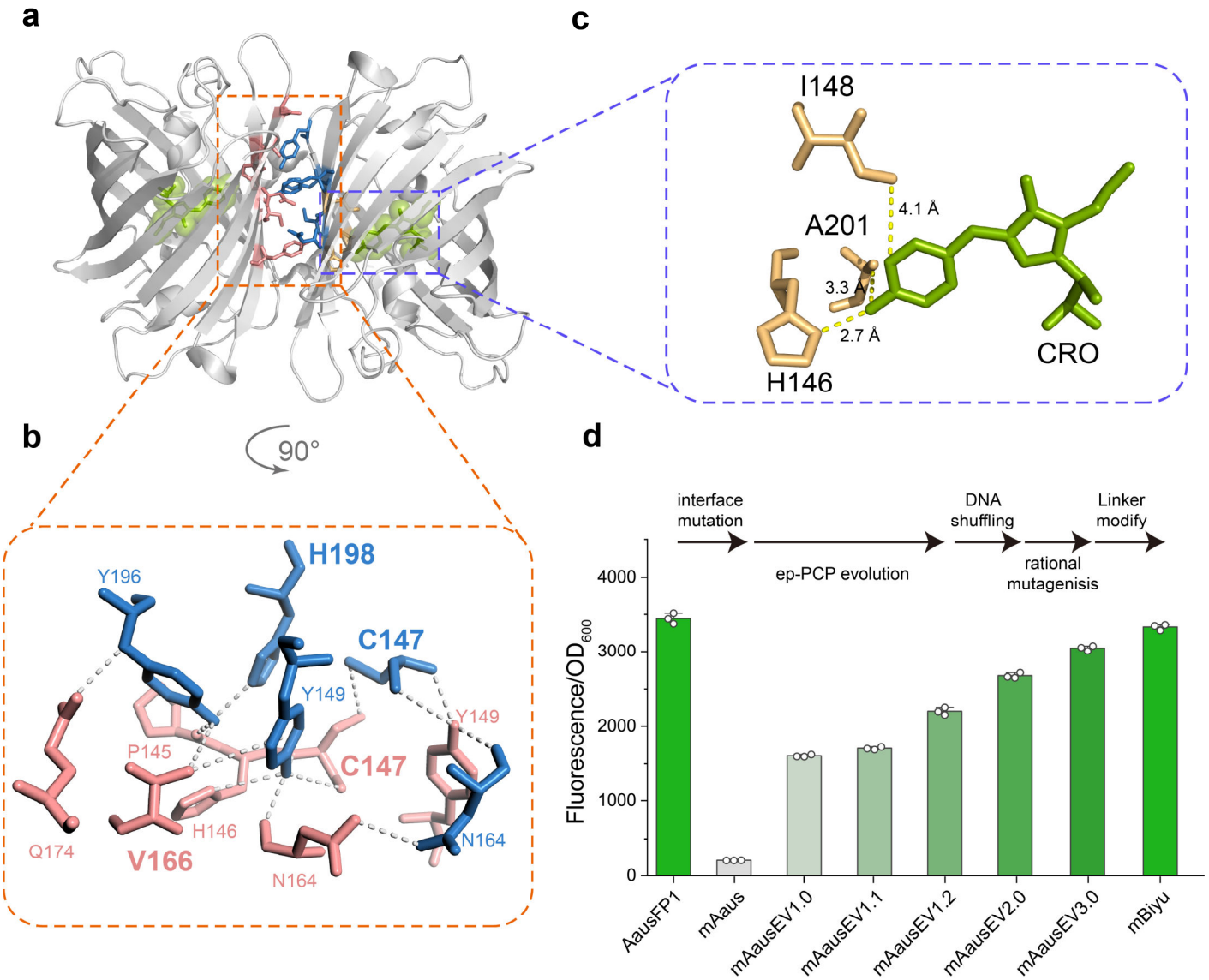

Figure 1 | Structure-guided engineering and directed evolution of mBiyu from AausFP1. a, Crystal structure of the AausFP1 dimer (PDB: 6S67), with chromophores shown in green and key residues at the dimer interface shown in teal-blue and pink. **b**, Residues at the dimer interface. Residues from the A protomer (left) are shown in pink and those from the C protomer (right) in teal-blue. C147, V166 and H198 for interface disruption are highlighted. **c,** Residues (light orange) in proximity to the chromophore (green). **d,** Relative fluorescence intensity (mean ± s.d.) of AausFP1 and representative variants obtained during the directed-evolution process. Fluorescence intensity of cell cultures was normalized to cell density (OD_{600}). Circles represent individual measurements (n = 3 replicates).

migrated exclusively as a monomer on pseudo-native SDS-PAGE and eluted as a single monomeric peak during size-exclusion chromatography (SEC) (Fig. S1b and c), indicating effective disruption of the dimer interface.

Directed evolution restores fluorescence of mAaus

Although mAaus was monomeric, it displayed severely reduced fluorescence in cultured bacterial cells (Fig 1d), indicating impaired folding and/or suboptimal chromophore maturation. To restore brightness while preserving monomericity, we implemented iterative directed evolution (Fig. S1a, Methods). We first performed error-prone PCR[12] to screen for colonies with high fluorescence. After three rounds, we obtained mAausEV1.2 with 64% of AausFP1 brightness recovery, harboring nine additional substitutions (T39A, P82L, A85T, L123M, Y143F, P145A, Q155E, I176R and Y196F) (Fig. 1d). Additional error-prone PCR rounds failed to yield further gains, suggesting that the variant had reached a local optimum in the fitness landscape.

To escape this local optimum, we recombined 10 brightest variants from the early rounds for DNA shuffling[13] (Fig. S1a, Methods). Using high-throughput flow-cytometric screening, we isolated a brighter variant mAausEV2.0, which recovered 78% of AausFP1 fluorescence (Fig. 1d). Comparing with mAausEV1.2, this variant gained A201T (near the chromophore), A178E, I148T and V103I, while T39A, L123M and Y196F were lost during recombination (Fig. S1a).

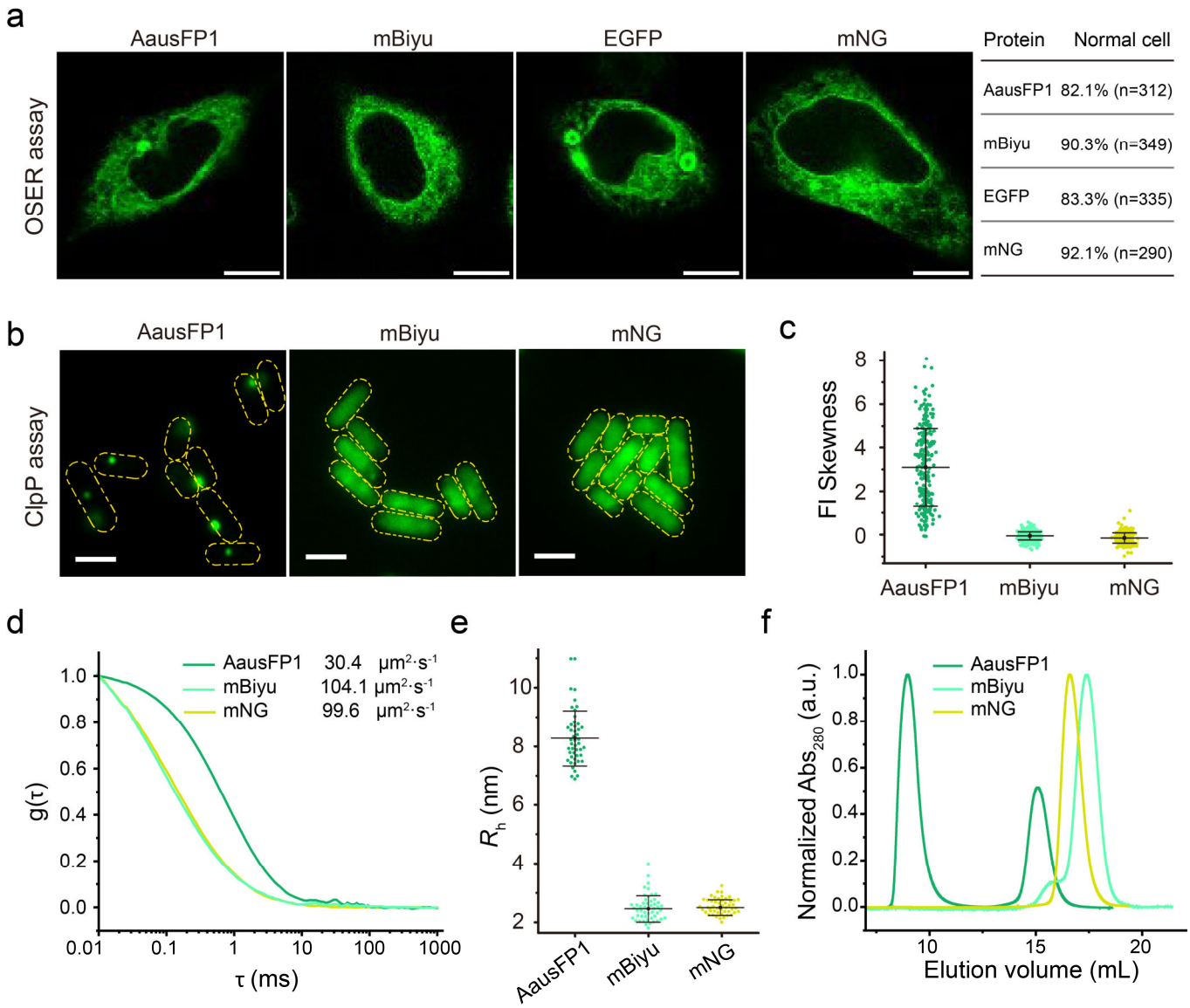

Figure 2 | Monomeric properties of mBiyu in vivo and in vitro. a, Representative images from the OSER assay of live HeLa cells expressing CytERM fused to AausFP1, mBiyu, EGFP, or mNG. Scale bars, 10 μm. Right: percentages of cells showing uniform CytERM distribution and the total number of cells analyzed (n). **b,** Representative images of *E. coli* cells expressing ClpP fused to AausFP1, mBiyu, or mNG (dashed outlines indicate cell boundaries). Scale bars, 2 μm. **c,** Skewness of fluorescence distribution in single cells shown in **b**. (n = 243, 500, 318 cells for AausFP1, mBiyu and mNG, respectively). **d,** Fluorescence autocorrelation curves of purified AausFP1, mBiyu and mNG (0.5 μM). Average diffusion coefficients (*D*) are indicated. **e,** Hydrodynamic radius (*Rh*) calculated from *D*. (n = 50 acquisitions per sample). **f,** Size-exclusion chromatography elution profiles of purified AausFP1, mBiyu and mNG. In **c** and **e**, data are shown as mean (lines) and s.d. (whiskers).

We also noted the emergence of I148T, also located at the dimer interface (adjacent to C147R) and proximal to the chromophore (Fig 1c), implicating a potential role in stabilizing the monomer and enhancing fluorescence.

Given the proximity to the chromophore, we next probed H146 (Fig. 1c) by saturation mutagenesis and revealed a clear brightness-photostability trade-off: H146C markedly increased photostability in *E. coli* (1.3-fold higher than mBaojin) but substantially reduced brightness (Fig. S2a and b), consistent with prior proposals that cysteine can enhance stability via oxidation-facilitated hydrogen bonding to the chromophore phenolate[14]. In contrast, H146S increased fluorescence ~2.5-fold while maintaining photostability comparable to mAausEV2.0 (Fig. S2a and b). During saturation mutation, we accidentally identified D168N which further improved the brightness, generating mAausEV3.0. Finally, adopting the N- and C-terminal peptides from mNeonGreen (mNG) improved brightness[15]. The resulting protein, designated mBiyu (Fig. S3), restored cell culture fluorescence to the level of AausFP1 in living *E. coli* cells (Fig. 1d).

mBiyu behaves as a monomeric in mammalian and bacterial cells

To evaluate whether mBiyu retains the monomeric state *in vivo*, we first assessed its behavior in mammalian cells using OSER assay[16]. CytERM-mBiyu was expressed in HeLa cells, and the fraction of transfected cells lacking whorled ER structures was 90.3% (n = 349). This percentage exceeded the commonly accepted threshold for monomericity[17], comparable to the monomeric control mNG (92.1%) and higher than AausFP1 (82.1%) or EGFP (83.3%) (Fig. 2a; Fig. S4a). In parallel, we examined aggregation propensity in *E. coli* by fusing FPs to ClpP[18,19]. Like ClpP-mNG, ClpP-mBiyu displayed homogenous cytosolic fluorescence indicating monomeric state, whereas ClpP-AausFP1 formed obvious puncta, consistent with poor solubility and aggregation (Fig. 2b and c).

We next characterized oligomeric state of mBiyu *in vitro*. Fluorescence correlation spectroscopy (FCS) showed that mBiyu diffused with a fast diffusion coefficient comparable to mNG whereas AausFP1 diffused more slowly (Fig. 2d). The calculated hydrodynamic radius (R_h) of mBiyu (2.5 ± 0.5 nm, mean ± s.d.) is similar to that of mNG (2.5 ± 0.3 nm, mean ± s.d.) and close the reported value of GFP monomer[20,21](Fig. 2e). Notably, AausFP1 exhibited a substantially larger R_h than a dimeric GFP, consistent with oligomerization observed by pseudo-native SDS-PAGE (Fig. S1b, Fig. S4b and c). Moreover, we validated that the mBiyu primarily stays in monomeric form at micro-molar concentration by size-exclusion chromatography and analytical ultracentrifugation (Fig. 2f and Fig. S4d).

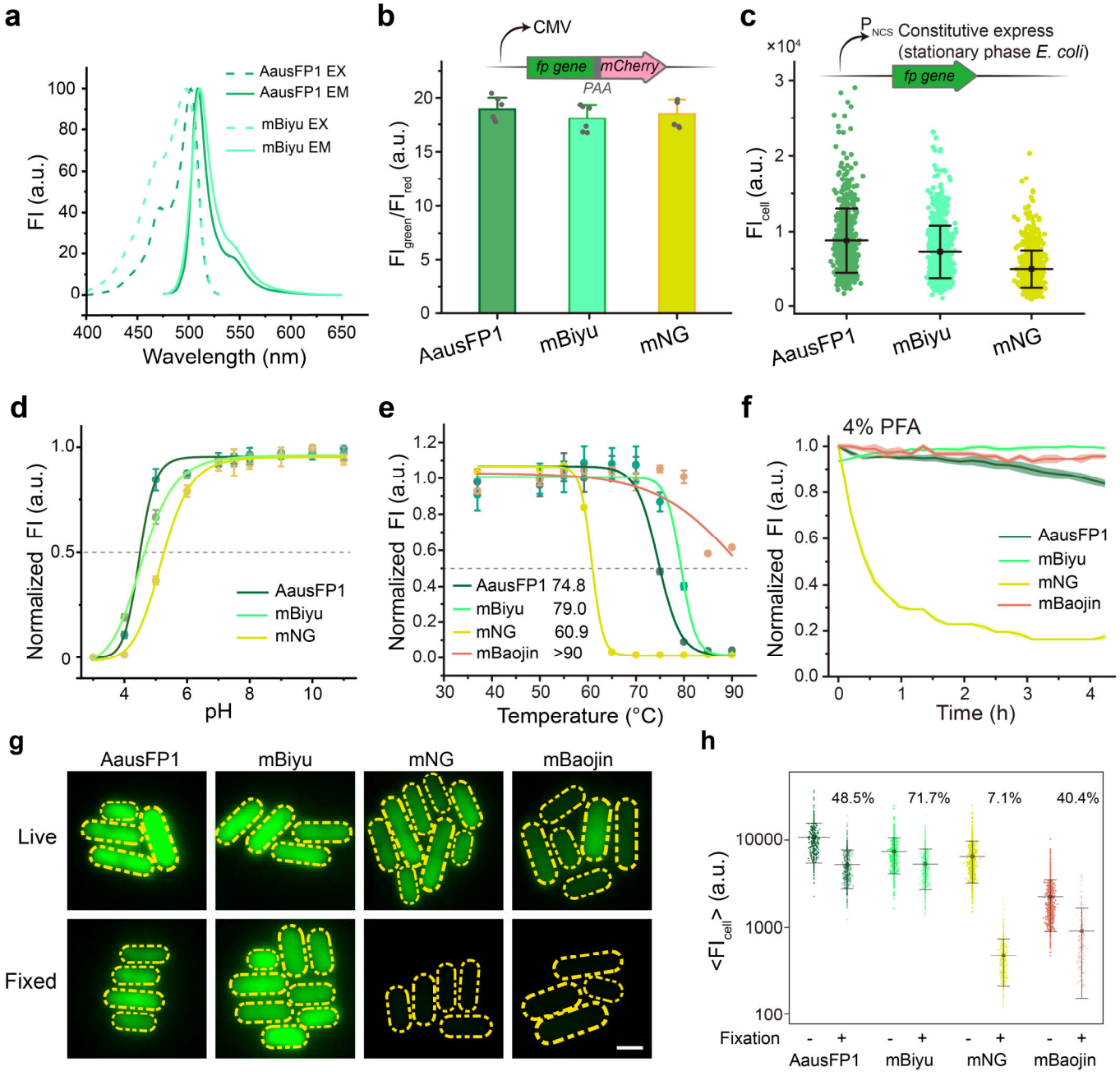

Figure 3 | Photophysical properties and stability of mBiyu. a, Excitation and emission spectra of AausFP1 and mBiyu. **b,** Green fluorescence intensity (FI) of AausFP1, mBiyu, and mNG, normalized to the corresponding red fluorescence of mCherry in single HeLa cells (6 experiments, > 10,000 cells per experiment). **c,** FI in single of *E. coli* cells (mean ± s.d., n = 610, 787, 832 cells for AausFP1, mBiyu and mNG, respectively). **d,** FI of purified FPs at different pH values, normalized to the maximum FI of each FP. **e,** FI versus temperature and fitted to a sigmoidal model. The melting temperature of each FP (T_m) is indicated. **f,** Decay of FI in *E. coli* cell cultures after fixation with 4% paraformaldehyde (PFA) at 25 °C. Data in **d**, **e**, and **f** are from three experiments and are shown as mean ± s.d. **g,** Representative images of *E. coli* cells before and after 2 h fixation using 4% PFA +5% glutaraldehyde (GLUT) at 25 ℃ followed by 2 d fixation at 4 ℃. Scale bars, 2 μm. **h,** Single-cell FI quantified from **g.** The percentages of fluorescence retained after fixation are in indicated for each FP. Means (lines) and s.d. (whiskers) are shown. (n (before/after fixation) = 369/559 (AausFP1), 480/623 (mBiyu), 539/509 (mNG), and 535/367 (mBaojin)).

mBiyu retained high brightness with chemical and thermal stability

Having established that mBiyu behaves as a monomer in living cells, we next characterized its photophysical and biochemical properties and benchmarked them against AausFP1, widely used monomeric green FP, mNG, and the recently developed photostable FP, mBaojin. Purified mBiyu exhibited a modest blue shift of the excitation maximum to 498 nm, better matched to common 488-490 nm laser lines than AausFP1 (502 nm) or mNG (505 nm) (Fig. 3a; Supplementary Table 2). Importantly, mBiyu retained a near-unity quantum yield (0.99). Although its extinction coefficient decreased relative to AausFP1, its molecular brightness is comparable with mNG (Supplementary Table 2).

We next evaluated the *in vivo* brightness in both mammalian and bacterial cells. In HeLa cells, co-expressing P2A-linked[22] mCherry with green FPs allowed ratiometric normalization to account for cell-to-cell expression variability. Under these conditions, mBiyu achieved 95.3% of AausFP1's cellular brightness, comparable to mNG (97.6%) (Fig. 3b). In *E. coli*, with expression from a constitutive promoter[6], mBiyu retained 81.0% of AausFP1 brightness and substantially outperformed mNG (56.2% of AausFP1) (Fig. 3c), indicating that mBiyu is a bright, monomeric FP suitable for both mammalian and bacterial applications.

Fluorescence lifetime imaging microscopy (FLIM) adds a time-domain contrast largely independent of probe concentration and excitation intensity, and is increasingly used in cellular imaging[23]. Fluorescent probes with single-exponential fluorescence decay greatly simplifies lifetime-based multiplexing and Förster resonance energy transfer (FRET) quantification[24]. Like mNG, mBiyu showed single-exponential decay in both time-resolved fits or phasor analysis (τ = 2.57 ± 0.04 ns), whereas AausFP1 and mBaojin exhibited multi-exponential behavior (Fig. S5a and b).

To assess performance of mBiyu under fixation or harsh conditions, we quantified its pH, chloride, thermal, and fixative tolerance. As its parental FP AausFP1, mBiyu displayed a low apparent pK_a of 4.6, indicating greater acid tolerant than mNG (Fig. 3d), and showed minimal sensitivity to chloride ions (Fig. S5c). These features are important for applications across different cell types and intracellular environments. Thermal stability assays (1-hour incubations at elevated temperatures) yielded an apparent T_m ~ 79.0 ºC of mBiyu, higher than AausFP1 and mNG (Fig. 3e), suggesting suitability for high-temperature workflows (e.g., rapid tissue clearing[25]) and thermophilic organisms[26]. We note that mBaojin also exhibited very high thermal stability (Fig. 3e).

Purified mBiyu also exhibited high resistance to aldehyde- and alcohol-based fixatives such as paraformaldehyde (PFA), glutaraldehyde (GUT), 70% Ethanol. mBiyu retained > 97% fluorescence after 4-h in 4%-PFA (Fig. 3f) or 4%-PFA+2%-GUT treatment (Fig. S5f), outperforming AausFP1 and mNG. After ethanol incubation, mBiyu and AausFP1 also showed higher fluorescence than mNG (Fig. S5d). After osmium tetroxide (OsO_4) incubation, only mBiyu showed detectable fluorescence (Fig. S5g). We further measured the remaining fluorescence in *E. coli* cells after 4% PFA + 5% GLUT fixation[27]. mBiyu retained 71.7% of its pre-fixation signal-the highest among tested FPs-compared with 48.5% for AausFP1 and 40.4% for mBaojin, while mNG retained only ~7.1% (Fig. 3g, h).

Collectively, the data indicate that mBiyu exhibits high brightness with single-exponential lifetime behavior and outstanding tolerance to chemical and thermal stresses, ensuring reliable performance across diverse circumstances and under harsh sample processing.

mBiyu folds and maturates rapidly, especially in bacterial cells

Another key property for fluorescent proteins is the speed of folding and chromophore maturation; faster maturation minimizes perturbation of the fusion partner and facilitate real-time imaging[28]. We therefore quantified the maturation kinetics by tracking the fluorescence intensity growth in live bacterial cultures after arresting translation with chloramphenicol[29]. AausFP1 matured rapidly with a half-time of 5.5 ± 0.3 min, whereas mBiyu was slightly slower (t_{50}= 9.4 ± 0.5 min), similar to mNG (t_{50} = 9.7 ± 0.7 min) and substantially faster than mBaojin (t_{50} = 35.1 ± 0.5 min) (Fig. 4a and b).

Notably, the maturation rate of mBaojin in *E. coli* was markedly slower than its originally reported *in vitro* rate ($t_{1/2}$=7.6 ± 2.4 min)[9]. We hypothesize that StayGold and its derivatives (e.g., StayGold-E138D[30] and mBaojin) mature substantially more slowly in reductive environment such as the cytoplasm of *E. coli*. Consistent with this, fluorescence of bacterial colonies expressing StayGold, StayGold-E138D, or mBaojin was lower than from colonies expressing AausFP1, mNG, or mBiyu after 15-hour incubation at 37 °C (Fig. 4c and d). mBaojin became brighter after an additional 1-3 days of maturation, whereas StayGold and StayGold-E138D remained dim (Fig S6a, b), indicating the StayGold-family variants are not optimal for live-cell imaging in reductive environment, particularly in some prokaryotes. This trend also held in the planktonic growing bacteria, where the fluorescence intensity of mBiyu and AausFP1 excessed that of mNG and mBaojin (Fig. S6c). Additionally, expression of mBaojin in *E. coli* (DH5α strain) hampered growth (Fig. S6d). These assays indicate that mBiyu is a strong candidate for prokaryotic imaging, a context historically underappreciated in FP development.

Therefore, we evaluated mBiyu as a fusion tag in representative bacterial organisms. First, we fused mBiyu to the essential peptidoglycan synthase PBP2 in the methicillin-resistant *Staphylococcus aureus* (MRSA, USA300 strain). Whereas sfGFP has been commonly used in *S. aureus*[31], PBP2-mBiyu produced markedly higher fluorescence and more distinct septal labeling (Fig. 4e, g). The signal was sufficient for time-lapse imaging of PBP2 dynamics, providing a practical route to study the cell biology of this clinically important pathogen (Fig. S7a, b; Movie S1). Second, we tested mBiyu in the mycobacterial model organism organisms, *Mycobacterium smegmatis*. Tagging the early division protein SepF with mBiyu showed clear division-ring localization (Fig. 4f). SepF-mBiyu exhibited higher fluorescence and a larger fraction of cells with assembled rings than SepF-mNG, whereas SepF-AausFP1 and SepF-mBaojin produced few detectable rings under the same conditions (Fig. 4f, h). Third, we tagged

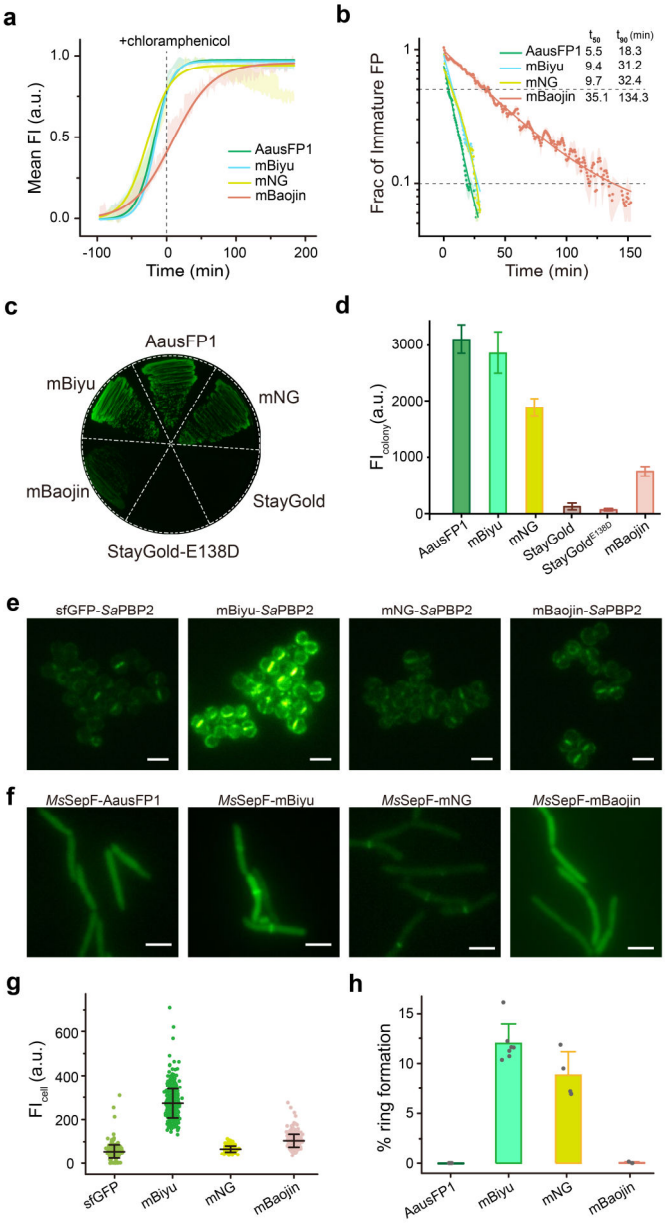

the core division protein FtsZ in *Escherichia coli*. FtsZ-mBiyu also generated division-ring signals stronger than FtsZ-mBaojin. Although FtsZ-AausFP1 produced even higher ring intensity, it induced abnormal ring architectures, consistent with perturbation from AausFP1 self-association (Fig S8a, b). Finally, we assessed performance of mBiyu in the extremophile bacterium, *Deinococcus radiodurans*. In this species, FtsZ-mBiyu produced brightest signals among all three FPs while maintaining the normal ring architecture (Fig. S8c, d).

Figure 5 | Performance of mBiyu fusions in mammalian cells. a-c, Representative fluorescence images of HeLa cells expressing H2B-AausFP1 and H2B-mBiyu. The white arrow indicates AausFP1 signal in the cytosol. Yellow arrows indicate H2B-AausFP1 aggregates in nucleus. **d-i**, Representative fluorescence images of HeLa cells expressing mBiyu fused α-tubulin (**d**), β-actin (**e**), keratin (**f**), ensconsin (**g**), Lifeact (**h**) and mitochondrial pre-sequence of human cytochrome c oxidase subunit VIII keratin (**i**). Scale bars, 10 μm.

Figure 4 | Performance of mBiyu in bacterial cells. a, Green fluorescence intensity (FI; normalized to the maximum) of *E. coli* cell cultures after translation arrest by chloramphenicol (n = 3 biological replicates; shaded regions, s.d.). **b,** Fractions of immature FP were calculated from the FI curves in **a** and fitted with exponential decay models to estimate two effective maturation times, t_{50} and t_{90}. **c,** Representative fluorescence image of *E. coli* colonies expressing six different FPs. **d,** Quantification of the single-colony FI in **c** (n = 3 biological replicates, mean ± s.d.). **e,** Representative fluorescence images of *S. aureus* cells expressing *Sa*PBP2-FP fusions. **f,** Representative fluorescence images of *M. smegmatis* cells expressing *Ms*SepF-FP fusions. **g,** Quantification of single-cell FI from **e** (n = 245, 521, 225, 404 cells for sfGFP, mBiyu, mNG and mBaojin, respectively). **h,** Percentage of detectable ring per micron of cell length from **f**, calculated by dividing the number of rings by the total length of counted cells (n = 114, 139, 94, 149 cells for AausFP1, mBiyu, mNG and mBaojin, respectively). **e** and **f**, scale bars, 2 μm.

Live-cell imaging and expansion microscopy with mBiyu

To evaluate performance in mammalian cells, we fused mBiyu to representative subcellular protein markers in HeLa cells. The original study identified AausFP1 reported that its histone H2B fusion (H2B-AausFP1) failed to localize to the nucleus, likely due to oligomerization[6]. In our experiments, H2B-AausFP1 showed both cytosolic and nucleus distribution yet formed bright puncta, consistent with aggregation behavior (Fig. 5a). By contrast, H2B-mBiyu showed uniform nuclear localization in both dividing and non-dividing cells, suggesting a functional fusion (Fig. 5b and c). We next fused mBiyu to α-tubulin, β-actin, keratin, and the microtubule-associated protein ensconsin; all fusions localized as expected in live cells (Fig. 5d-g). LifeAct-mBiyu also clearly labeled the filament network of F-actin without detectable cytoskeletal disorganization (Fig. 5h). Additionally, the mitochondrial pre-sequence of human cytochrome c oxidase subunit VIII (COX8) fused to mBiyu enabled the observation of mitochondria in living-Hela cells (Fig. 5i). These results show that mBiyu serves as a reliable fusion tag for diverse proteins in mammalian cells.

Because mBiyu is highly resistant to formaldehyde-based fixation and proteinase K (Fig. S5e), we next tested its compatibility with

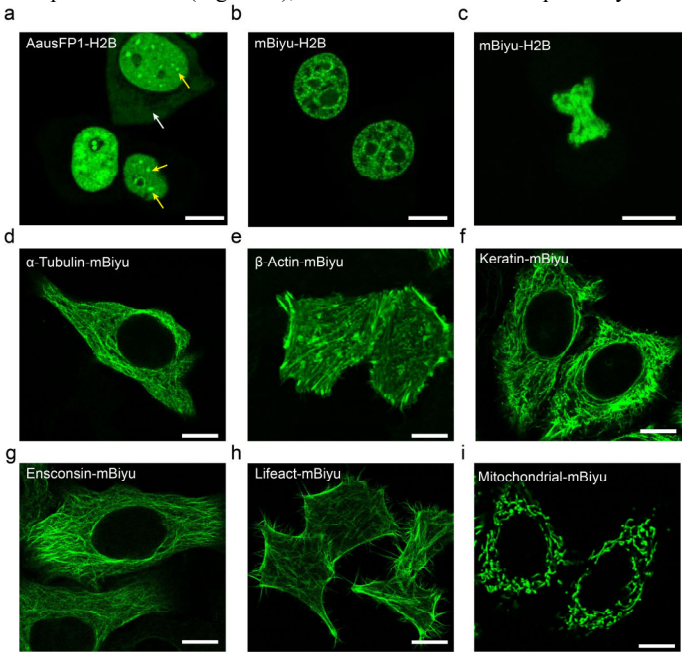

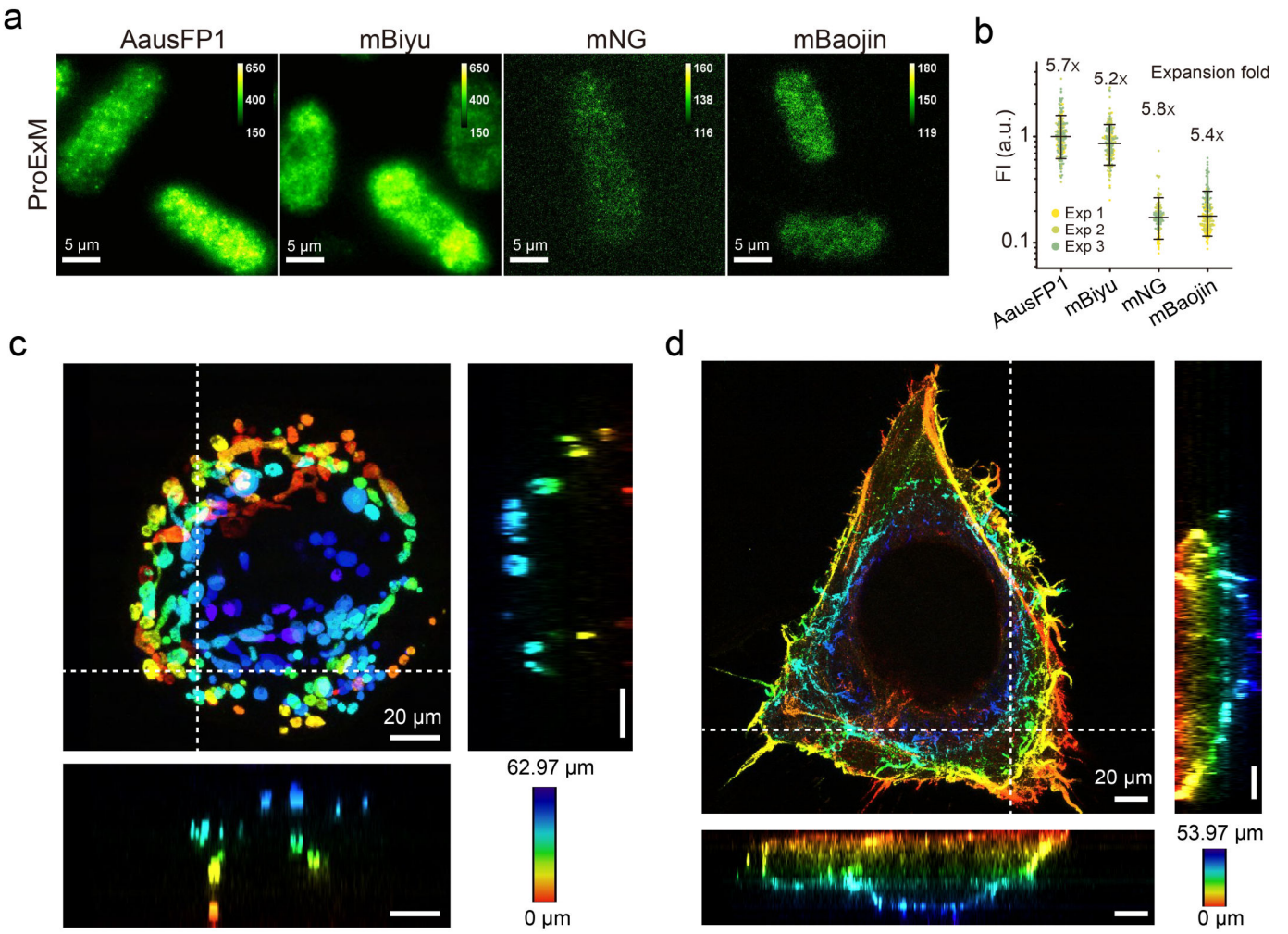

Figure 6 | mBiyu in expansion microscopy. a, Representative images of *E. coli* cells expressing AausFP1, mBiyu, mNG, and mBaojin after expansion. Scale bars, 5 μm. **b**, Quantification of single-cell fluorescence intensity from **a**. FI is normalized to mean intensity of AausFP1 within each replicate (n = 50-100 cells per replicate). Mean FI (lines) and s.d. (whiskers) are shown. **c,** Representative proExM image of mitochondria of a Hela cell labeled by mBiyu. **d,** Representative proExM image of Lifeact-mBiyu in a Hela cell. **c-d,** color indicated the z axis. Scale bars, 20 μm.

expansion microscope[32]. We first quantified the fluorescence retention of four FPs in expanded bacterial cells using a modified protein retention ExM (ProExM)[33] workflow (Fig 6a, Methods). Cell expressing AausFP1 retained clear cytoplasmic fluorescence even after the hydrogel embedding and proteinase K treatment, reaching a 5-fold expansion (Fig S9). Notably, mBiyu showed higher fluorescence (84% of AausFP1), substantially exceeding the other two monomeric FPs, mNG (17.2%) and mBaojin (19.3%) (Fig 6b, Fig S9c). Considering the monomeric property, mBiyu serves the best choice in ProExM among the tested FPs. We further tested the performance of mBiyu in ProExM of mammalian cell. Hela cells with mBiyu fused to COX8 or LifeAct exhibited high signal-to-noise ratio after expansion (linear expansion factor: 7.09 ± 0.30, mean ± s.d., n = 3 replicates) and depicted the subcellular structure of mitochondrial (Fig. 6c, Fig. S10a, b) and F-actin filaments (Fig. 6d, Fig. S10c, d).

Discussion

AausFP1 is among the brightest green fluorescent proteins reported to date, but its strong tendency to oligomerize has limited its use as a functional fusion tag. Here we engineered mBiyu, a monomeric derivative of AausFP1 that preserves high brightness while behaving as a monomer under physiological conditions (Fig. 2a-c). mBiyu also matures rapidly, particularly in prokaryotic hosts such as *Escherichia coli*, *Staphylococcus aureus*, and *Deinococcus radiodurans*. It tolerates harsh processing, including acidic environments, aldehyde fixation, and protease treatment (Fig. 3d-h and Fig. S5e). Together, these properties make mBiyu well suited for demanding workflows, including live-cell imaging in difficult organisms and organelles, as well as super-resolution approaches such as expansion microscopy (Fig. 6).

AausFP1 and mBiyu exhibit exceptional resistance to chemical and thermal stress relative to many commonly used green FPs. One likely contributor is the intrinsic stability of the AausFP1 β-barrel and its chromophore environment, which may prevent solvent and reagent access and suppress unfolding or chromophore-destabilizing pathways. In addition, the mutated residues in mBiyu (Fig. S3a) may have reinforced general structure stability that made it more resistant to heat and chemical fixation. While the precise structural determinants remain to be elucidated, these results suggest that AausFP1-derived variants

occupy an unusually stable region of FP sequence space.

Beyond intrinsic photophysics, mBiyu is particularly valuable as a fusion tag in bacteria. In our tests, StayGold-family FPs exhibited markedly slow maturation in bacterial cells (Fig. 4c, d), likely reflecting constraints imposed by the more reductive cytoplasmic environment, which limits their utility for real-time bacterial imaging. In contrast, mBiyu performed robustly across diverse prokaryotes and enabled high-contrast time-lapse imaging of essential proteins in pathogenic bacteria and extremophile bacteria, such as *S. aureus*, *M. smegmatis*, and *D. radiodurans* (Fig.4e-h and Fig. S8). This capability opens opportunities to extend advanced imaging methods to clinically relevant organisms where reliable FP options have been limited, with potential to accelerate mechanistic studies relevant to antimicrobial strategies.

mBiyu performs strongly across hosts and conditions and also outlines clear opportunities for further development. Structural insight into how interface disruption reshapes the chromophore environment could guide computational design to increase the extinction coefficient and further boost brightness. Photostability may be improved through targeted substitutions (e.g., at H146) (Fig. 1c and Fig. S2). In addition, mBiyu provides a foundation for spectrally shifted variants for multicolor imaging and lifetime-tuned derivatives for multiplexed FLIM. Most importantly, expanding the repertoire of well-characterized, non-avGFP-derived sequences such as mBiyu should aid data-driven and AI-assisted FP design by enriching training space with distinct photophysical solutions.

Methods

Plasmid construction

Unless otherwise noted, plasmids were assembled by PCR amplification of fragments followed by one-step isothermal cloning (ClonExpress Ultra One Step Cloning Kit V2, Vazyme). Primer sequences and plasmids are provided in Supplementary Table 3 and Supplementary Table 4.

Bacterial expression plasmids.

***E. coli*:** pNCST-*aausfp1* plasmid[6] was synthesized by Genewiz based on the sequence of pNCST (Addgene #129499). pNCSY backbone was derived from pNCST with the pMB1 origin replaced by the p15A origin (from pXY421[34]) to reduce constitutive expression level. DNA fragments encoding FP genes were amplified from pNCST (*aausfp1*), pXY421 (*mng*), and pBADHisB-*sumo-mbaojin*[9] and cloned into the pNCSY backbone, generating expression plasmid of AausFP1 (pYY196), mNG (pYY197) and mBaojin (pYY270). For expressing *Ec*FtsZ-FP fusions in *E. coli*, *EcftsZ* gene amplified from pXY027[35] was assembled with *aausfp1*, *mng*, *mbaojin* or *mbiyu* via sequence encoding polypeptide linker0 (GGGGSPAPAPGGGGS) and cloned to the pZH509 backbone[36], generating plasmids pYY298 (*EcftsZ-mng*), pYY299 (*EcftsZ-aausfp1*), pYY260 (*EcftsZ-mbaojin*), pYY414 (*EcftsZ-mbiyu*). Plasmids encoding *EcclpP-fp* (pYY391, pYY392, pYY393, pYY415) was constructed as *Ec*FtsZ fusions, but with an SGGGG polypeptide linker. The *clpP* gene was amplified from *E. coli* K12 MG1655 genomic DNA

S. aureus: pCN5 backbone (pSJ197) was derived from pCNX plasmid (a gift from the Pinho Lab[37]) by replacing its Kan^R cassette to Cam^R cassette and promoter region to P_{spac} (IPTG inducible). The DNA fragments bearing Cam^R cassette and P_{spac} promoter were amplified from pHW205 and pHW101 respectively. For expressing FP-*Sa*PBP2 in *S. aureus*, *Sapbp2* gene amplified from pSJ197 was assembled with codon-optimized *mbaojin* or *mbiyu* (synthesized by Genewiz) and cloned into the pCN5 backbone, generating pYY451 (pCN5-*mbaojin-Sapbp2*) and pYY452 (pCN5-*mbiyu-Sapbp2*).

M. smegmatis: pLY528 backbone was derived from pKW08-lx (Addgene #25012) by removing the *luxA* and *luxB* genes. For expressing *Ms*SepF-FP in *M. smegmatis*, *MsspeF* gene amplified from the genomic DNA of WT *MS* strain (mc^2155) was assembled with *aausfp1*, *mng*, *mbaojin* or *mbiyu* via sequence encoding GA-linker (GAGAGSGAGAGS) and cloned to pLY528 backbone, generating pLX190 (pLY528-*MssepF-aausfp1*), pLX177 (pLY528-*MssepF-mbaojin*), pLX178 (pLY528-*MssepF-mbiyu*) and pLX179 (pLY528-*MssepF-mng*).

D. radiodurans: For expressing *Dr*FtsZ-FP in *D. radiodurans*, *DrftsZ* gene amplified from the genomic DNA of WT *DR* strain (R1) was assembled with *aausfp1*, *mng*, *mbaojin* or *mbiyu* via sequence encoding linker0 and cloned to pJWK[38] backbone, generating pYY457 (pJWK-*DrftsZ-aausfp1*), pYY458 (pJWK-*DrftsZ-mng*), pYY459 (pJWK-*DrftsZ-mbiyu*), pYY460 (pJWK-*DrftsZ-mbaojin*).

Mammalian expression vectors.

OSER constructs: The pCytERM backbone was amplified from pYS001 (pCytERM-*demono*[39]) and assembled with codon-optimized *aausfp1*, *mng*, *egfp* and *mbiyu* genes (synthesized by CENCEFE Biotech), generating pYY443 (pCytERM-*aausfp1*), pYY444 (pCytERM-*mng*), pYY445 (pCytERM-*egfp*), pYY446 (pCytERM-*mbiyu*).

H2B and LifeAct fusion constructs: The dsDNA fragments encoding *mbiyu* and *aausfp1* were amplified from pYY446 and pYY443 and cloned into the pcDNA3.1(+) backbone to generate pYY482 (pcDNA3.1(+)-*mbiyu-h2b*), pYY485 (pcDNA3.1(+)-*aausfp1-h2b*) and pYY483 (pcDNA3.1(+)-*lifeact-mbiyu*).

Other mBiyu fusion vectors: *mbiyu* gene amplified from pYY446 was cloned into corresponding vectors made by Han et al[9]. to replace the original *mbaojin* gene (Supplementary Table3), generating pYY494 (pcDNA-*mbiyu-tubulin*), pYY495 (pN1-*emtb-mbiyu*), pYY496 (pAAV-*dmito2-mbiyu*), pYY497 (pN1-*mbiyu-actin*), and pYY498 (pN1-*keratin-mbiyu*).

Mutagenesis and library screening

Random mutagenesis was performed by error-prone PCR[40] (Random Mutagenesis Kit, Beyotime). Mutation rates were tuned by varying the amount of template input and mutation enhancer to achieve low (0-4.5 mutations·kb^{-1}) or medium (4.5-9 mutations·kb^{-1}) rates. Site-saturation mutagenesis was introduced using a pool of primers containing NNK codons using p520 kit Vazyme). DNA shuffling was performed by staggered extension recombination[41] using the plasmids with top 1-5 brightest fluorescence from each round (in the first DNA shuffling, three variants showed strongest monomericity were added). Reassembly reactions were allowed for 80 cycles (95 °C for 30 s; 55 °C for 15 s) with *Taq* DNA polymerase (Takara).

dsDNA fragments encoding mutagenized FP genes were cloned into pNCSY backbone downstream of the TEV protease cleavage site. *E. coli* DH5α cells were transformed with the resulted plasmids or library and plated on LB-agar with 50 μg·mL^{-1} carbenicillin and incubated at 37 °C for 12 h.

For each round, ~5,000-15,000 colonies (10-30 plates) were screened using a fluorescence imaging system (SH-523, Shenhua Science Technology) equipped with 470/20 nm excitation filter and 530/20 nm emission filter. The ~20 brightest colonies were re-streaked and further evaluated for oligomeric state by pseudo-native SDS-PAGE assay. The green fluorescence intensity of the cell cultures of monomeric variants with the same cell density (OD600 ~ 3) were then measured on a microplate reader with 460 - 480 nm excitation and 505 -

525 nm emission (Spark, Tecan). The brightest variant served as the template for the subsequent round of mutagenesis, while the top 8 or 12 variants were chosen for the next round of DNA shuffling. In total, seven rounds of error-prone PCR, one round of site-saturation mutagenesis, and two rounds of DNA shuffling were performed (Fig S1a).

Protein expression and purification

Recombinant fluorescent proteins were expressed in *E. coli* DH5α carrying pNCSY-*fp* plasmids with the semi-constitutive promoter[6]. Overnight cultures were grown in 500 mL 2×YT medium with carbenicillin (50 μg·mL⁻¹) at 37 °C with shaking (220 rpm). Proteins were purified by Ni-NTA affinity chromatography (QIAGEN) and dialyzed overnight against TBS (50 mM Tris-HCl (pH 8.0) buffer supplemented with 150 mM NaCl).

Pseudo-native SDS-PAGE

Bacterial pellets from 1 mL overnight culture were lysed on ice for 2 h using BugBuster Master Mix (Merck Millipore). The lysates were then separated on 12% polyacrylamide gels under pseudo-native conditions as described previously[42].

Size-exclusion chromatography

SEC was performed on a Superdex™ 200 10/300 GL column (Cytiva) on an ÄKTA™ purifier system. Protein samples were eluted in TBS buffer as above at a flow rate of 0.5 ml/min and detected by a 280-nm detector. Fractions were collected in 1-mL aliquots using an automated fraction collector (Cytiva) for downstream experiments.

Analytical Ultracentrifugation (AUC)

Sedimentation velocity was measured on a Beckman Optima AUC analytical ultracentrifuge at 20 °C, following a 1-h thermal equilibration at 0 rpm. For each run, protein solution (2 μM; 400 μL) and TBS buffer (410 μL) were loaded into 12-mm double-sector cells. Rotor speeds were 30,000 rpm (AausFP1) or 50,000 rpm (mNG and mBiyu), selected based on expected molecular masses[43]. The time-dependent radial absorbance profiles were monitored using a UV-Vis detector (230 nm or 280 nm) and analyzed with SEDFIT (version 15.01b[44]) to determine the continuous sedimentation coefficient distribution, c (s). Buffer density and viscosity were estimated using Sednterp[45].

Fluorescence Correlation Spectroscopy (FCS)

FCS experiments were performed on a commercial bench-top fluorescence correlation spectrometer (CorTectorTM SX200, LightEdge Technologies Limited) equipped with a 60X 1.2NA UPLANSAPO water immersion objective ((Olympus). Fluorescence was excited by a 488-nm laser and filter with an ET525/50m filter (Chroma) using a single-photon counting avalanche photodiode detector (SPCM-800-14-FC, Excelitas). Purified proteins were diluted to 500 nM in PBS. Autocorrelation curves, $G(\tau)$, were recorded every 2 s for 50 repetitions per sample at 25 °C. Each $G(\tau)$ was fitted with the 3D diffusion model including a triplet term:

$$G(\tau) = \frac{1}{N}\left(1+\frac{\tau}{\tau_D}\right)^{-1}\left(1+\frac{\tau}{S^2\tau_D}\right)^{-\frac{1}{2}}\left(1+\frac{T}{1-T}e^{-\frac{\tau}{\tau_T}}\right)$$

where N is the average number of fluorescent molecules in the observation volume, τ_D is the diffusion time, S is the structure parameter (ratio of axial to radial dimensions of the confocal volume), T is the triplet fraction, and τ_T is the triplet correlation time. The diffusion coefficients of FPs were calibrated using a 10 nM ATTO488 carboxyl acid solution (ATTO-TEC GmbH, Siegen) ($D = 4.26 \times 10^{-6}\ cm^2\ s^{-1}$) under identical conditions. The hydrodynamic radius (Rh) was then derived from the Stokes-Einstein equation:

$$R_h = \frac{k_B T}{6\pi\eta D}$$

where k_B is the Boltzmann constant, T is the absolute temperature (298 K), and η is the buffer viscosity (assumed to be that of water at 25 °C, 0.89 mPa·s).

Quantum yield (QY) and extinction coefficient (EC)

Relative QY was determined as described previously[46]. Fluorescent proteins (in TBS) and fluorescein standard (in 0.1 M NaOH, QY = 0.95) were diluted to an absorbance between 0.05 and 0.1 at 460 nm, respectively. Absorbance spectra (220-650 nm) were acquired on a U-3900/3900H spectrophotometer (Hitachi High-Tech). Emission spectra (475-650 nm; 0.2 nm step; excitation 460 nm) were acquired on an F-7100 fluorescence spectrophotometer (Hitachi High-Tech). Quantum yield was calculated using the established method as follow[46]:

$$\Phi_{FP} = \Phi_{STD}\left(\frac{k_{FP}}{k_{STD}}\right)\left(\frac{n^2{}_{FP}}{n^2{}_{STD}}\right)$$

where Φ_{STD} is the quantum yield of the standard (0.95), k_{FP} and k_{STD} are the slope of the linear fit for the integrated fluorescence intensity of the fluorescent protein as a function of absorbance, respectively. n_{FP} and n_{STD} are the refractive indices of the fluorescent protein and the standard solutions, respectively.

EC were determined by alkaline denaturation method[47]. Fluorescent proteins in TBS were mixed 1:1 with 2 M NaOH solution. The denatured chromophore has ε = 44,000 M^{-1} cm^{-1} in 1 M NaOH[48].

Maturation kinetics

Maturation kinetics were measured using a translation-arrest assay[29]. *E. coli* DH5α expressing FPs were grown overnight in LB medium (1% Tryptone, 0.5% yeast extract, 1% NaCl, Oxoid) at 37 °C, diluted 1:100 into 96-well clear-bottom black plates (LABSELECT), and monitored green fluorescence intensity and OD_{600} every 2 min at 37 °C (Spark Tecan). Once OD_{600} reach 0.2, chloramphenicol was added (final concentration:150 μg·mL^{-1}) to halt translation. The fluorescence increase from maturation of pre-synthesized FPs was tracked. Maturation curves were calculated as described previously[29].

Cellular cytotoxicity in bacteria

To assess the impact of FP expression on *E. coli* growth, stationary-phase cultures were diluted 1:100 in LB medium and OD_{600} were recorded every 2 min for 20 hours at 37 °C (Spark Tecan). Wild-type DH5α strain (no plasmid) served as a growth control.

Cellular brightness in Hela cells

HeLa cells were transfected with pcDNA3.1(+)-AausFP1-P2A-mCherry, pcDNA3.1(+)-mNG-P2A-mCherry, or pcDNA3.1(+)-mBiyu-P2A-mCherry plasmids using Lipofectamine 3000 (Invitrogen). After 48 h, cells were harvested and resuspended in cold Phosphate-buffered saline (PBS). Flow cytometry was performed on a CytoFLEX (BECKMAN COULTER), acquiring more than 100,000 events per sample. Green FPs was excited at 488 nm and detected with a 525/40 nm emission filter, while mCherry was excited at 561 nm and detected with a

585/42 nm emission filter. Mean green fluorescence was normalized to the mean mCherry fluorescence to determine the effective cellular brightness.

pKa determination

Buffers with pH from 3.0 to 11.0 were prepared as described previously[6]. Purified protein was diluted to 1 μM in each buffer and immediately transferred to 96-well clear-bottom black plates to measure the green fluorescence intensity immediately (Spark, Tecan). pKa values were obtained by fitting the data to a sigmoidal dose-response curve.

Thermodynamic stability

Purified FPs were diluted to 1 μM in TBS, incubated for 1 h at temperatures ranging from 37 °C to 90 °C, and cooled to room temperature. The green fluorescence intensity was measured as above using microplate reader (Sparker Tecan). Melting temperatures (T_m) were determined as the half-intensity temperature of the corresponding sigmoidal fitting curve.

Chemical and enzymatic stability

For salt tolerance, purified FPs were diluted to 1 μM in TSB containing 0-0.8 M NaCl. For protease resistance, purified FPs (1 μM, TBS) were incubated with 8 U·mL^{-1} Proteinase K (NEB) at room temperature. For fixative tolerance, *E. coli* cells expressing FPs were fixed with 70% ethanol (Macklin) or 4% paraformaldehyde (PFA, Electron Microscopy Sciences). All diluted samples were immediately transferred to 96-well black plates to monitor the green fluorescence intensity for 3-4 h at room temperature (Spark Tecan).

For fixative tolerance, *E. coli* cells expressing FPs were fixed with 4% paraformaldehyde and 5% glutaraldehyde for 2 h at RT followed by 2 days at 4 ℃., washed three times with PBS, and observed under wide-field microscopy (**Wide-field imaging section**). Live-cell samples without fixation were imaged under the same laser power and camera setups for comparison. Cell ROIs were segmented using CellposeSAM[49] to extract the mean fluorescence intensity (MFI) of each cell.

Microscopy

Sample preparation:

Live bacterial sample were prepared as previously described for wide-field and confocal imaging[38]. Briefly, the *E. coli* cells carrying pNCSY-*fp* were grown overnight in LB medium at 37 ℃ and diluted into fresh LB medium (Oxoid) for an additional 4-h incubation. Cells were washed three times with PBS and applied on a pre-made 1.5% agarose gel pad (PBS). For fixation, cell cultures were washed three times with PBS and incubated in 4% PFA for 10 min at 25 ℃ followed by 1.5 h at 4 ℃. After fixation, cells were washed three times with PBS and applied on the gel pad for imaging. For *E. coli* pZH509-*clpP-fp* strains, the log-phase cell culture (OD_{600} ≈ 0.2) was induced with 10 nM anhydrotetracycline (ATc) in M9 minimal medium (M9) at 25 °C for 5 h before applying on the gel pad for imaging. For *E. coli* pZH509-*EcftsZ-fp* strains, log-phase cell culture in M9 medium was used for imaging without induction. For *S. aureus* pCN5-*fp-Sapbp2* strains, the cells were cultured in tryptic soy broth (TSB, Difco) at 37 °C to an OD_{600} ≈ 0.03 and induced with 0.5 mM isopropyl β-D-1-thiogalactopyranoside (IPTG) for 2 h. For *M. smegmatis* strains bearing pLY528-*MssepF-fp* were cultured in 7H9 medium (Difco) at 37 ℃ to an OD_{600} ≈ 0.5 without induction. Cells were washed three times with PBS and applied on a pre-made 2% agarose gel pad (ultrapure water). For *D. radiodurans,* strains bearing pJWK-*DrftsZ-fp* were cultured in 2×TGY medium (1% Tryptone, 0.2% Glucose, 0.6% Yeast extract, Oxoid) at 30°C to an OD_{600} ≈ 0.4 and induced with 5 nM ATc for 3 h.

For expansion microscopy, 4% PFA fixed *E. coli* cell cultures were further fixed with 70% ethanol for 15 min at 25 °C followed by 2.5-h incubation at 4 °C, then washed with cold PBS (4 °C). The pellet was resuspended in PBS to OD_{600} ≈ 2.5 and incubated with mutanolysin (400 U ml^{-1}, Sigma) and murine RNase inhibitor (0.1 U μL^{-1}, Vazyme) for 2 h at 37 °C. Glass coverslips (24× 40 mm, Thermo Fisher Scientific) were cleaned by ultrasonication and plasma cleaner (TS-PL10, TONSON) and coated with 100 μg mL^{-1}Poly-D-lysine (Sigma) for at least 6 h at 25 °C and washed three times with DEPC-treated water. Proteins in the samples were relevantly anchored by 5% acrylate glycidyl ether (AGE; TCI) dissolved in 100 mM $NaHCO_3$ (Aladdin) for 1 h at 25 °C in the dark, followed by three washes with PBS. Hydrogels were prepared according to the Bacterial-MERFISH formulation[50]. Single-use 980 μL aliquots of gel solution (1.1 M sodium acrylate, 2 M acrylamide and 60 ppm bis-acrylamide; Sigma) were prepared and stored at -20°C. Before polymerization, 10% ammonium persulfate (APS; Macklin) and 10% TEMED (Macklin) stock solutions were added to final concentrations of 0.1% each. Gel chambers were assembled using Repel-Silane-treated microscope slides (25 x 75 mm, Citotest) and 0.15 mm spacers. Polymerization was performed for 2 h at 25 °C under nitrogen environment. Hydrogels were incubated overnight at 37 °C in digestion buffer containing 50 mM Tris pH 8.0 (Sangon Biotech), 1 mM EDTA (Aladdin), 0.5% Triton X-100 (Aladdin), and 0.8 M NaCl (Biofroxx), supplemented with Proteinase K (8 U·mL^{-1}). Gels were transferred to excess nuclease-free water to initiate expansion and incubated for 30 min per round with water replacement. This step was repeated three times to achieve full expansion. Expanded gels were trimmed and mounted onto Poly-D-lysine-coated slides.

Live Hela cells were transfected with plasmids encoding FPs targeted to H2B, actin, tubulin, keratin, microtubules, mitochondria, or the endoplasmic reticulum (ER) using Lipofectamine 3000. Cells were cultured in Dulbecco's modified Eagle medium (DMEM) supplemented with 10% fetal bovine serum (FBS), 0.5% penicillin-streptomycin, and 50 μM β-mercaptoethanol (all from Invitrogen) at 37 °C in a humidified 5% CO_2 incubator. Cells were seeded onto 35-mm glass-bottom dishes (Greiner Bio-One) for 48 h before imaging (24 h for ER constructs). For expansion microscopy, transfected Hela cells were cultured as described above and seeded onto Poly-D-lysine-treated glass coverslips. At 48 h, cells were fixed with 4% PFA for 15 min at 25 °C and washed three times with PBS. Subsequent anchoring, gel embedding, digestion and expansion were performed as described above for bacterial samples with minor modifications: The anchor step was performed at 37 °C for 2 h, and digestion was performed at 37 °C for 4 h.

Confocal and fluorescence lifetime imaging

The confocal imaging of Hela cells and lifetime imaging of *E. coli* cells were performed on a Leica STELLARIS 8 confocal microscope equipped with an HC PL APO CS2 100×/1.4 NA oil-immersion objective. Images were acquired with a zoom factor of 1.0 and a pinhole size of 1.0 Airy unit (151.7 μm at 580 nm). Excitation power of 488 nm was set to 2% and the emission fluorescence between 500 nm and 550 nm using a HyD S 2 detector (gain of 2.5).

Wide-field imaging

Wide-field imaging was performed on a custom-built wide-field microscope consisting[51] of a Nikon Ti2-E inverted body with a 100×/1.49 NA TIRF objective and a Prime BSI sCMOS camera (Teledyne Photometrics). Excitation was provided by a 488-nm laser

(OBIS) using highly inclined and laminated optical sheet (HILO) illumination[52]. Emission was collected through a ZT488rdc dichroic mirror and a 525/50 nm band-pass filter (Chroma Technology). The focal plane was positioned in the middle of the cells. For time-lapse imaging, frames were acquired every 10 min for up to 4 h with an exposure time of 100 ms. Microscope control and data acquisition were managed using custom software (Beijing Dawkhosin Technology). For photostability assay, the sample was continuously illuminated with relatively high laser power (9.4 W cm^{-2} or 5.5 W cm^{-2}); images were acquired every 5 s (20 ms exposure) for 10 min.

Imaging of *M. smegmatis* was acquired using an Olympus BX53 upright microscope equipped with a Retiga R1 camera (QImaging), a CoolLED pE-4000 light source, and a U Plan XApochromat phase-contrast objective (100×/1.45 NA). Green fluorescence was imaged using the Chroma EGFP filter set EGFP/49002.

Data analysis

The fraction of cells exhibiting normal ER morphology in the OSER assay was quantified as described previously[16].

Fluorescence lifetime data were processed using Leica FLIM software. The emission photon counts were adjusted below 2000 per pixel. The decay curves were fitted with either single-exponential (mNG and mBiyu) or double-exponential (AausFP1 and mBaojin) models based on χ^2 values and phasor plot analysis.

Expansion microscopy image processing for HeLa cells:

Raw images were processed using a modified sparse deconvolution algorithm[53]. The denoising and reconstruction procedure was formulated as:

$$\arg\min_{g}\left\{\frac{\text{fidelity}}{2}|f-g|_2^2+hessian(|\partial_{xx}g|_1+|\partial_{yy}g|_1+|\partial_{xy}g|_1 +|\partial_{yx}g|_1+sparsity\cdot|g|_1\right\}$$

where f represents the raw fluorescence image containing low background and high-frequency noise, and g is the denoised and reconstructed output. The three parameters-fidelity, Hessian regularization, and sparsity-control the trade-off between denoising and signal preservation. In this study, these parameters were set to 150, 10, and 15, respectively.

Denoised images were then stacked and subjected to drift correction using StackReg (FIJI plugin; translation mode, https://bigwww.epfl.ch/thevenaz/stackreg/). For depth-encoded visualization, the Z-stack was processed using the ZstackDepthColorCode v.0.0.2 plugin ((https://github.com/UU-cellbiology/ZstackDepthColorCode) with the "physics" lookup table (LUT), and the corresponding color bar was generated. Three-dimensional reconstruction and animation were generated using Imaris 9.2, with a total of 100 frames per rendering.

Data availability

Data are available on request from the lead contact.

Acknowledgments

The authors thank other members in Yang, Chen, and Du's laboratory for their valuable advice and discussions with special thanks to Xinci Wang for assistance with microscope setup and imaging and Di Yan for assistance with plasmid construction and Ruijiao Liu for preserving strains. The authors thank Dr. Kiryl D. Piatkevich, Dr. Jiangliu Yu, Dr. Xiuhong Hu, Dr. Mariana Pinho, and Dr. Zach Hensel for providing bacteria strains and plasmids, thank Lihao Ding for providing fluorescein. The authors thank Guoyun Liu, Zhenzhou Wang, Dr. Hongwu Qian, Dr. Lin Xue for helpful suggestions and discussions. The authors thank for Dr. Zhangyi Liang for insightful discussion. The authors would like to acknowledge Dr. Haiyan Liu for providing CytoFLEX SRT. The authors would like to acknowledge the Confocal Imaging Unit at the Core Facility Centre for Life Science, University of Science and Technology of China. The Laboratory research staff (Zhenbang Liu, M.S.) contributed valuable technical expertise and assistance to this project. This work was supported by the National Natural Science Foundation of China (32270035 to X.Y., 32550762 to Q.C., and 32270049 to S.D.), the Center for Advanced Interdisciplinary Science and Biomedicine of IHM (BJ9100000056 to X.Y. and QYPY20230035 to Q.C.), the Fundamental Research Funds for the Central Universities WK9100000063 to X.Y., and the USTC start-up funding (KY9100000035, KJ2070000083 to X.Y.).

Author Contributions

Conceptualization: Y.Y., Q.C., X.Y.
Methodology: Y.Y., C.P., X.Y, X.O., Y.L., S.D., Q.C., X.Y.
Investigation: Y.Y., Y.S., C.P., X.W., X.L., J.W., S.Z., H.W., X.Y.,
Software: X.O.,
Formal analysis: Y. Y., X. Y.
Writing – original draft: Y.Y., X.Y.
Writing – review & editing: Y.Y., C.P., X.Y., Y.L., S.D., Q.C., X. Y.
Supervision: Q.C., X. Y.
Funding acquisition: S.D., Q.C., X. Y.

Declaration of interests

The authors declare no competing financial interest.

Additional Information

Lead contact:

Information and requests for reagents may be directed to, and will be fulfilled by, the lead contact, Xinxing Yang (xinxingyang@ustc.edu.cn).

Materials availability:

Strains and plasmids are available on request from the lead contact with a materials transfer agreement.

Correspondence:

Correspondence should be addressed to Quan Chen (chenquan@ustc.edu.cn) and Xinxing Yang (xinxingyang@ustc.edu.cn).

Supplementary Information:

Supplementary Information is available for this paper.

References

1 Shimomura, O., Johnson, F. H. & Saiga, Y. Extraction, purification and properties of aequorin, a bioluminescent protein from the luminous hydromedusan, *Aequorea*. *J Cell Comp Physiol* **59**, 223-239 (1962).

2 Cormack, B. P., Valdivia, R. H. & Falkow, S. FACS-optimized mutants of the green fluorescent protein (GFP). *Gene* **173**, 33-38 (1996).

3 Pédelacq, J. D., Cabantous, S., Tran, T., Terwilliger, T. C. & Waldo, G. S. Engineering and characterization of a superfolder green fluorescent protein. *Nat Biotechnol* **24**, 79-88 (2006).

4 Shaner, N. C. *et al.* Improving the photostability of bright monomeric orange and red fluorescent proteins. *Nature Methods* **5**, 545-551 (2008).

5 Hirano, M. *et al.* A highly photostable and bright green fluorescent protein. *Nature Biotechnology* **40**, 1132-1142 (2022).

6 Lambert, G. G. *et al.* *Aequorea*'s secrets revealed: New fluorescent proteins with unique properties for bioimaging and biosensing. *PLoS Biol* **18**, e3000936 (2020).

7 Shaner, N. C., Steinbach, P. A. & Tsien, R. Y. A guide to choosing fluorescent proteins. *Nat Methods* **2**, 905-909 (2005).

8 Shaner, N. C. *et al.* A bright monomeric green fluorescent protein derived from *Branchiostoma lanceolatum*. *Nature Methods* **10**, 407-409 (2013).

9 Zhang, H. *et al.* Bright and stable monomeric green fluorescent protein derived from StayGold. *Nat Methods* **21**, 657-665 (2024).

10 Schrodinger, LLC. The PyMOL Molecular Graphics System, Version 4.6. PyMOL (2015).

11 Campbell, R. E. *et al.* A monomeric red fluorescent protein. *Proceedings of the National Academy of Sciences* **99**, 7877-7882 (2002).

12 Wilson, D. S. & Keefe, A. D. Random mutagenesis by PCR. *Curr Protoc Mol Biol* **Chapter 8**, Unit8.3 (2001).

13 Crameri, A., Whitehorn, E. A., Tate, E. & Stemmer, W. P. Improved green fluorescent protein by molecular evolution using DNA shuffling. *Nat Biotechnol* **14**, 315-319 (1996).

14 Ren, H. *et al.* Cysteine Sulfoxidation Increases the Photostability of Red Fluorescent Proteins. *ACS Chemical Biology* **11**, 2679-2684 (2016).

15 Shaner, N. C. *et al.* Improved monomeric red, orange and yellow fluorescent proteins derived from *Discosoma* sp. red fluorescent protein. *Nature Biotechnology* **22**, 1567-1572 (2004).

16 Costantini, L. M., Fossati, M., Francolini, M. & Snapp, E. L. Assessing the Tendency of Fluorescent Proteins to Oligomerize Under Physiologic Conditions. *Traffic* **13**, 643-649 (2012).

17 Cranfill, P. J. *et al.* Quantitative assessment of fluorescent proteins. *Nature Methods* **13**, 557-562 (2016).

18 Landgraf, D., Okumus, B., Chien, P., Baker, T. A. & Paulsson, J. Segregation of molecules at cell division reveals native protein localization. *Nature Methods* **9**, 480-482 (2012).

19 Fraikin, N., Couturier, A., Mercier, R. & Lesterlin, C. A palette of bright and photostable monomeric fluorescent proteins for bacterial time-lapse imaging. *Science Advances* **11**, eads6201 (2025).

20 Ormö, M. *et al.* Crystal structure of the *Aequorea victoria* green fluorescent protein. *Science* **273**, 1392-1395 (1996).

21 Teijeiro-Gonzalez, Y. *et al.* Time-Resolved Fluorescence Anisotropy and Molecular Dynamics Analysis of a Novel GFP Homo-FRET Dimer. *Biophysical Journal* **120**, 254-269 (2021).

22 Liu, Z. *et al.* Systematic comparison of 2A peptides for cloning multi-genes in a polycistronic vector. *Scientific Reports* **7**, 2193 (2017).

23 Tan, Z. *et al.* Time-resolved fluorescent proteins expand fluorescent microscopy in temporal and spectral domains. *Cell* **188**, 6987-7005.e6928 (2025).

24 Goedhart, J. *et al.* Bright cyan fluorescent protein variants identified by fluorescence lifetime screening. *Nature Methods* **7**, 137-139 (2010).

25 Xiong, H. *et al.* A highly stable monomeric red fluorescent protein for advanced microscopy. *Nature Methods* **22**, 1288-1298 (2025).

26 Pulschen, A. A. *et al.* Live Imaging of a Hyperthermophilic Archaeon Reveals Distinct Roles for Two ESCRT-III Homologs in Ensuring a Robust and Symmetric Division. *Curr Biol* **30**, 2852-2859.e2854 (2020).

27 Campbell, B. C., Paez-Segala, M. G., Looger, L. L., Petsko, G. A. & Liu, C. F. Chemically stable fluorescent proteins for advanced microscopy. *Nature Methods* **19**, 1612-1621 (2022).

28 Gadella, T. W. J. *et al.* mScarlet3: a brilliant and fast-maturing red fluorescent protein. *Nature Methods* **20**, 541-545 (2023).

29 Balleza, E., Kim, J. M. & Cluzel, P. Systematic characterization of maturation time of fluorescent proteins in living cells. *Nature Methods* **15**, 47-51 (2018).

30 Ivorra-Molla, E. *et al.* A monomeric StayGold fluorescent protein. *Nature Biotechnology* **42**, 1368-1371 (2024).

31 Rondthaler, S. N., Sarker, B., Howitz, N., Shah, I. & Andrews, L. B. Toolbox of Characterized Genetic Parts for *Staphylococcus aureus*. *ACS Synthetic Biology* **13**, 103-118 (2024).

32 Chen, F., Tillberg, P. W. & Boyden, E. S. Expansion microscopy. *Science* **347**, 543-548 (2015).

33 Tillberg, P. W. *et al.* Protein-retention expansion microscopy of cells and tissues labeled using standard fluorescent proteins and antibodies. *Nat Biotechnol* **34**, 987-992 (2016).

34 Yang, X. *et al.* A two-track model for the spatiotemporal coordination of bacterial septal cell wall synthesis revealed by single-molecule imaging of FtsW. *Nature Microbiology* **6**, 584-593 (2021).

35 Buss, J. *et al.* A multi-layered protein network stabilizes the *Escherichia coli* FtsZ-ring and modulates constriction dynamics. *PLoS Genet* **11**, e1005128 (2015).

36 Hensel, Z. A plasmid-based *Escherichia coli* gene expression system with cell-to-cell variation below the extrinsic noise limit. *PLoS One* **12**, e0187259 (2017).

37 Monteiro, J. M. *et al.* Cell shape dynamics during the staphylococcal cell cycle. *Nature Communications* **6**, 8055 (2015).

38 Wang, J. *et al.* Class A PBPs reinforce the septal cell wall following initial synthesis by SEDS–bPBP pairs during bacterial cytokinesis. Preprint at https://biorxiv.org/content/10.1101 (2025).

39 Hu, X. *et al.* Using Protein Design and Directed Evolution to Monomerize a Bright Near-Infrared Fluorescent Protein. *ACS Synthetic Biology* **13**, 1177-1190 (2024).

40 McCullum, E. O., Williams, B. A., Zhang, J. & Chaput, J. C. Random mutagenesis by error-prone PCR. *Methods Mol Biol* **634**, 103-109 (2010).

41 Zhao, H., Giver, L., Shao, Z., Affholter, J. A. & Arnold, F. H. Molecular evolution by staggered extension process (StEP) *in vitro* recombination. *Nature Biotechnology* **16**, 258-261 (1998).

42 Yanushevich, Y. G. *et al.* A strategy for the generation of non-aggregating mutants of Anthozoa fluorescent proteins. *FEBS Lett* **511**, 11-14 (2002).

43 Schuck, P., Zhao, H., Brautigam, C. A. & Ghirlando, R. *Basic principles of analytical ultracentrifugation* (CRC Press Boca Raton, FL, 2016).

44 Schuck, P. Size-Distribution Analysis of Macromolecules by Sedimentation Velocity Ultracentrifugation and Lamm Equation Modeling. *Biophysical Journal* **78**, 1606-1619 (2000).

45 Philo, J. S. SEDNTERP: a calculation and database utility to aid interpretation of analytical ultracentrifugation and light scattering data. *Eur Biophys J* **52**, 233-266 (2023).

46 Wall, K. P., Dillon, R. & Knowles, M. K. Fluorescence quantum yield measurements of fluorescent proteins: A laboratory experiment for a biochemistry or molecular biophysics laboratory course. *Biochemistry and Molecular Biology Education* **43**, 52-59 (2015).

47 Subach, F. V. *et al.* Photoactivatable mCherry for high-resolution two-color fluorescence microscopy. *Nature Methods* **6**, 153-159 (2009).

48 Chudakov, D. M. *et al.* Photoswitchable cyan fluorescent protein for protein tracking. *Nature Biotechnology* **22**, 1435-1439 (2004).

49 Pachitariu, M., Rariden, M. & Stringer, C. Cellpose-SAM: superhuman generalization for cellular segmentation. Preprint at https://biorxiv.org/content/10.1101 (2025).

50 Sarfatis, A., Wang, Y., Twumasi-Ankrah, N. & Moffitt, J. R. Highly multiplexed spatial transcriptomics in bacteria. *Science* **387**, eadr0932 (2025).

51 Yan, D., Xue, J., Xiao, J., Lyu, Z. & Yang, X. Protocol for single-molecule labeling and tracking of bacterial cell division proteins. *STAR Protocols* **5**, 102766 (2024).

52 Tokunaga, M., Imamoto, N. & Sakata-Sogawa, K. Highly inclined thin illumination enables clear single-molecule imaging in cells. *Nature Methods* **5**, 159-161 (2008).

53 Zhao, W. *et al.* Sparse deconvolution improves the resolution of live-cell super-resolution fluorescence microscopy. *Nature Biotechnology* **40**, 606-617 (2022).